Proceedings of the ASME 2024
18th International Conference on Energy Sustainability
ES2024
July 15 – 17, 2024, Anaheim, CA

ES2024-131343

A REINFORCEMENT LEARNING-BASED HIERARCHICAL SPEED CONTROL OF AN INFINITELY VARIABLE TRANSMISSION FOR TIDAL CURRENT ENERGY CONVERTERS

Zhichang Qin
School of Mechanical Engineering
Tianjin University of Technology
Tianjin, 300384, China

Gang Li
Michael W. Hall School of Mechanical Engineering
Mississippi State University
Starkville, MS, 36762

Weidong Zhu*
Department of Mechanical Engineering
University of Maryland Baltimore County
Baltimore, MD, 21250

ABSTRACT

A tidal current energy converter (TCEC) is a device specifically designed to harness the kinetic energy present in tidal energy and convert it into stable mechanical rotational energy, which can then be used to generate electricity. The core component of the TCEC is an infinitely variable transmission (IVT), which adjusts the speed ratio to maintain a stable output speed regardless of the input speed changes caused by tidal changes. In order to ensure the efficient driving performance of the IVT system, a closed-loop control strategy based on IVT state measurement data is studied in this paper. This method can effectively track the expected output speed of the IVT system in general TCEC. Based on the proposed speed control strategy, the speed regulation of the whole IVT system under different conditions is studied in theory and simulation. These promising results could directly contribute to future research to improve the efficiency of tidal energy harvesting.

Keywords: Tidal current energy harvesting; Infinitely variable transmission; Data-driven control; Output speed regulation

NOMENCLATURE

Roman letters

i	Speed ratio of the IVT
x	State vector
t	Time point
j	Time step
x_0	Initial value of the state vector
f, g	Unknown dynamics of the DC motor
J	Cost function
H	Hamilton function
V	Value function
Q, R	Matrices that define the Lagrange function
q	Number of the data points that used to train NNs

Greek letters

ω_t	Rotation speed of the CFTs
ω_p	Input speed of the IVT
ω_u	Output speed of the IVT
ω_n	Input speed of the noncircular gear
λ_{tsr}	Optimal TSR value value of the CFts
τ_p	Input torque of the IVT
λ_{tsr}	Optimal TSR value value of the CFts
θ_n	Rotation angular of the second noncircular gear
$\theta_{sg1}, \theta_{sg2}$	Rotation angular of the solar wheel in two planetary gear systems
θ_s	Rotation angular of the control shaft
ω_u^*, ω_n^*	Desired values of ω_u, ω_n
$\hbar$	Boundary function of the crank length
λ_p, λ_i	Proportional gain and integral gain of the crank length controller
Δ_{ω_u}	Tracking error of the output speed of the IVT
$\mathcal{L}$	Lagrange function
μ	Lagrange multiplier

Dimensionless groups

r_{og}	Pitch radius of the output gear
ℓ_{cr}	Crank length of the IVT
i_n	Speed ratio of the noncircular gear pair
$\ell_{cr\max}$	Maximum value of the crank length
ℓ_{cr}^*	Desired crank length
V_p	Armature voltage of the DC motor
u_p	Control voltage applied to the DC motor
u_p^*	Optimal control input
u_p'	Admissible control input
$\mathbf{W}_V$	Coefficient matrix of the critic neural network
$\mathbf{W}_u$	Coefficient matrix of the actor neural network

Superscripts and subscripts

k	Iteration number

*Corresponding author: wzhu@umbc.edu

1. INTRODUCTION

Oceans cover 72% of the earth's surface and contain vast sources of renewable energy [1]. However, most ocean energy technologies are in their early stages of development, from concept design to demonstration [2]. Tidal current energy converters (TCECs) are devices designed to capture the kinetic energy of tidal flows [3]. Currently, TCECs require a current speed higher than 2.25 m/s, which corresponds to water depths between 25 and 50 m to produce practical power [4]. This requires larger swept areas of turbine blades and high tidal current speeds. However, only less than 2% of sea regions with high-tidal current speeds can satisfy the existing tidal current harvesting systems[5]. If the cut-in speed of a TCEC is too low, the corresponding speed ratio of the gear transmission must be very small to harvest enough tidal energy. Therefore, a variable speed ratio transmission that costs less and has more efficiency needs to be used for TCECs under low-speed and high-torque conditions[6].

The IVT system, as described in [7, 8], consists of three main components: a motion conversion module (MCM), an input control module (ICM), and a non-circular gear pair. The schematic diagram of the IVT system is shown in Figure 1. The input power from the prime mover is transmitted to the ICM through the meshing of the active and driven non-circular gears. Within the ICM, there are two planetary gear sets with identical structures. The control action generated by the stepper motor is transmitted through two gears mounted on the control shaft and the idler shaft, ultimately influencing the motion of the crank in the MCM. The output speed of the ICM is first converted to the translation speed of the Scotch yoke mounted on the MCM. Then, the translation speed is converted to the speed of the four output gears on the output shaft through the four rack-pinion meshing. The speed of the four output gears is corrected by one-way bearings and transmitted to the output shaft as the output speed of the IVT.

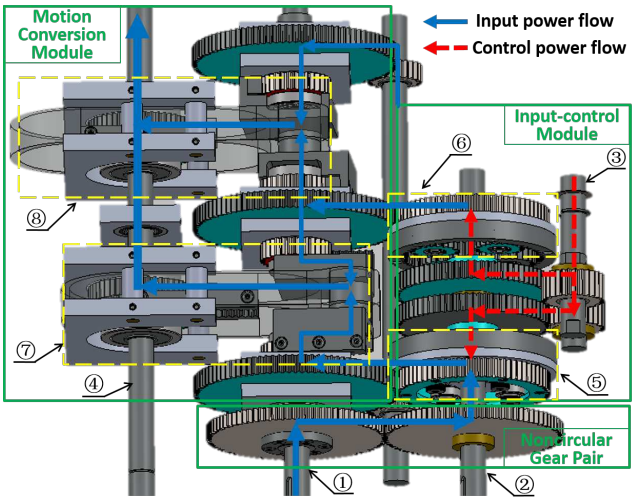

FIGURE 1: SCHEMATIC DRAWING OF THE IVT [7], WHERE 1 IS THE INPUT SHAFT, 2 IS THE SECONDARY SHAFT, 3 IS THE CONTROL SHAFT, 4 IS THE OUTPUT SHAFT, 5 IS THE FIRST PLANETARY GEAR SET (PGS), 6 IS THE SECOND PGS, 7 IS THE FIRST SCOTCH-YOKE SYSTEM (SYS), AND 8 IS THE SECOND SYS.

The IVT is a unique transmission system that uses contact forces instead of friction to transfer torque, making it suitable for both low and high torque conditions. It has a broader range of variable speed ratios compared to continuously variable transmissions (CVTs), and it can be started from zero. The main objective of the IVT control system is to optimize the crank length to achieve high operating performance in TCECs. To achieve this goal, a nonlinear closed-loop speed ratio control method combined with integral delay feedback control has been developed and described in [8]. This control method allows the IVT to adjust its speed ratio to the desired output speed with any variable input speed. By incorporating delay control, the speed fluctuation of the IVT output speed is significantly reduced, resulting in more accurate speed ratios. The control strategy has been successfully implemented in the IVT system, and experimental results have demonstrated the IVT's potential for broad application in TCECs.

It is important to note that the control approach put forward in [9, 10] for the IVT system is model-based. This means that a mathematical model of the IVT system must be established based on its physical mechanism before the control design process can begin. However, the accuracy of model-based control design methods is strongly influenced by the accuracy of the dynamical model. Because the IVT components often have nonlinear, uncertain, and complex dynamics, it is often challenging to establish an exact dynamical model and accurately identify its parameters. In recent years, there has been a growing interest in using data science to actively control complex systems [11, 12]. The data-based control design approach reduces the dependence on system dynamics models, and it may not even require any model information at all. This paper proposes a new speed control method for the IVT system based on reinforcement learning. This approach enables accurate speed control without establishment of a dynamic model of the IVT system for tidal current energy converters. We highlight the contributions of this paper as follows:

(i) combining the crank length controller and an RL-based data-driven speed controller, we put forward a near-optimal hierarchical speed control framework for the IVT system in tidal current energy applications; and

(ii) without establishing the dynamic model of the IVT system, the control algorithm can track the output speed of the IVT system accurately by using only the input and output data of the system.

The paper is structured as follows. In Sect. 2, we introduce an IVT-based TCEC system. We then present the theoretical design of a crank length controller based on the IVT's physical mechanism in Sect. 3. Next, in Sect. 4, we propose a data-driven RL-based speed controller for the DC motor system, which is based on the sampling input-output data of the system. To demonstrate the feasibility of the proposed control strategy, we provide a special scenario case about IVT control design for a TCEC in Sect. 5. Finally, we conclude the paper in Sect. 6.

2. IVT-BASED TCEC SYSTEM

In the TCEC system, two hybrid Darrieus modified-Savonius cross-flow turbines (CFTs), an IVT, and a doubly-fed induction generator are used, as shown in Fig. 2. These CFTs have a

unique design that combines a modified Savonius-type turbine in the central region and a Darrieus-type turbine in the outer region. This design is known to enhance the hydrodynamic performance of the entire turbine system by combining the advantages of the Darrieus configuration and the modified Savonius configuration [13]. The IVT receives the input speed of the CFTs, which is determined based on the tip-speed ratio (TSR) of the CFTs that can be written as

$$\omega_t = \omega_p = \frac{\lambda_{tsr} v_{tidal}}{r_t} \tag{1}$$

where v_{tidal} is the tidal speed, $r_t = 2$ m is the CFT' rotor diameter, and $\lambda_{tsr} = 2$ is the optimal TSR value under the highest energy harvesting efficiency of CFTs at low and high tidal speed [14]. The torque τ_p applied to the IVT input shaft is equal to the output

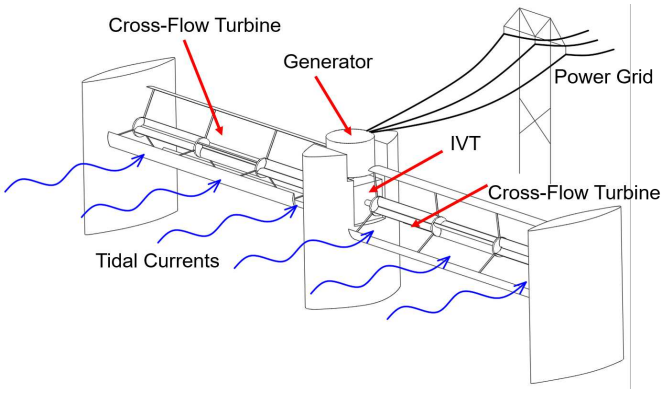

FIGURE 2: SCHEMATIC DRAWING OF THE IVT-BASED TCEC [10].

torque provided by the two CFTs under the action of the tidal forces. However, in practice, it is difficult to calculate this torque accurately, and usually, a torque sensor is used to measure it. The output rotation speed of the IVT, denoted as ω_u, determines the speed ratio of the IVT, defined as $i = \frac{\omega_p}{\omega_u}$, where ω_p is the rotation speed of the IVT input shaft. The torque τ_u applied to the IVT output shaft depends on the motion of its loads, such as the type of generator and the output power.

The second noncircular gear (NG2) rotates with a period of 2π and has a rotation angle denoted by θ_n. The modulated rotation speed of the ICM, represented by ω_n, is the rotation speed of NG2 and can be calculated as $\omega_n = \frac{\omega_p}{i_n}$, where $i_n = \frac{\pi}{2\sqrt{2}} \max\left\{\sin\theta_n, \sin(\theta_n - \frac{\pi}{2}), \sin(\theta_n - \pi), \sin(\theta_n - \frac{3\pi}{2})\right\}$ is the speed ratio of the noncircular gear pair. Based on the kinematic model of the IVT described in [9, 10], the speed ratio of the IVT can be expressed as

$$i = \frac{\omega_p}{\omega_u} = \frac{\sqrt{2}\pi r_{og}}{4\ell_{cr}} \tag{2}$$

In the design of the IVT system, the pitch radius of the output gear is set as 38.1 mm, while the speed ratio is determined by the length of the crank, denoted as ℓ_{cr}. Specifically, the crank length is proportional to the difference between the rotation angles of the solar wheel in the two planetary gear systems, divided by four, i.e., $\ell_{cr} = \frac{\theta_{sg1} - \theta_{sg2}}{4}$. As the two control gears rotate in opposite directions with equal magnitudes, we have $\theta_{sg1} = -\theta_{sg2}$, and hence the speed ratio of the IVT is adjusted by the rotation angle θ_{sg1} of the first control gear, which is equivalent to the rotation angle θ_s of the control shaft.

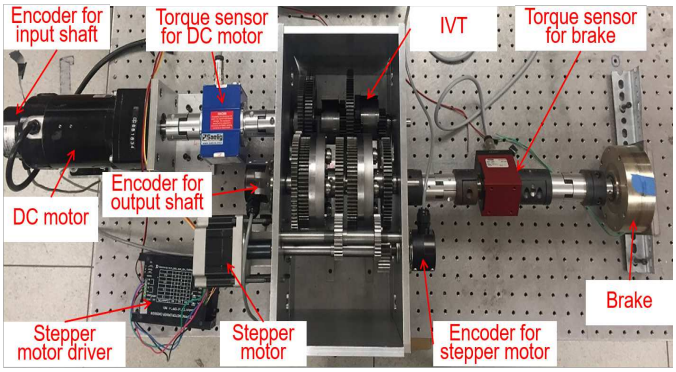

FIGURE 3: THE EXPERIMENTAL SETUP OF THE IVT SYSTEM [9].

It is essential to note that the dynamic performance of the IVT system depends on the states of the input shaft and the crank length. Therefore, the control behavior and the speed ratio vary with the input speed, which is the unknown time-varying tidal velocity, and the rotation angle θ_s of the control shaft. As a result, the primary control objective of the IVT-based TCEC is to design a control algorithm that can achieve the desired speed output of the IVT system under these changing conditions. To achieve this objective, the control algorithm should be able to adapt to the varying input speed and the rotation angle of the control shaft. Hence, it should be designed to provide a robust and accurate control performance. This approach will ensure that the IVT-based TCEC system can operate smoothly and maintain a stable speed output, despite the changes in input conditions.

In the IVT-based TCEC system, the output speed of the turbine is utilized as the input speed of the IVT. However, for laboratory experiments, a direct current (DC) motor is used instead of the hydraulic turbine to drive the IVT and study its control problem. The experimental setup, shown in Fig. 3, comprises an IVT, a DC motor, a magnetic brake, a stepper motor, two torque sensors, and three angular encoders. The DC motor generates output shaft speeds that satisfy the relationship described in Eq. (1) and drives the IVT to operate. The control speed of the control gears is provided by a stepper motor. The magnetic brake mounted on the output shaft provides a variable load for the IVT system. Three angular encoders mounted on the input shaft, the output shaft, and the control shaft of the IVT measure their rotation angles. To achieve the primary control goal of IVT-based TCEC, the output speed ω_u of the IVT needs to converge to a desired output speed ω_u^* by adjusting the crank length ℓ_{cr} when the DC motor operates at the rotation speed of the hydro-turbine.

To achieve this control objective, two controllers work in tandem to form the hierarchical speed control of the IVT-based TCEC. The first controller, the crank length controller, generates a desired crank length ℓ_{cr}^* based on the speed ratio of the desired input speed ω_n^* and the output speed ω_u^* required in the IVT system. The second controller, the data-driven optimal speed

controller [12], forces the modulated input speed ω_n of the ICM to approach the desired input speed ω_n^*. By working together, these two controllers can achieve the desired output speed of the IVT system and ensure a stable and efficient operation of the TCEC system.

Overall, the laboratory setup provides a convenient and controlled environment for studying the control problem of the IVT-based TCEC system. By using the DC motor as the input, researchers can investigate the system's dynamic behavior and evaluate different control strategies for achieving the desired output speed under varying input conditions.

3. CRANK LENGTH CONTROLLER

The hierarchical speed control system for the IVT-based TCEC comprises two critical control strategies: the crank length forward control and the crank length feedback control. The crank length forward control calculates the desired crank length ℓ_{cr}^* based on Eq. (2). This control strategy is designed to ensure that the output speed of the IVT system converges to the desired output speed. Specifically, the desired crank length is given by

$$\ell_{cr}^* = \frac{\sqrt{2}\pi r_{og}\omega_u^*}{4i_n\omega_n^*} \tag{3}$$

The physical limit of the crank length is taken into account by developing a look-up table based on the maximal crank length $\ell_{cr\,\max}$. If $\ell_{cr}^* \le \ell_{cr\,\max}$, then the crank length used in the IVT system is a function of the desired modulated input speed ω_n^* and the desired output speed ω_u^*, i.e., $\ell_{cr}(\omega_n^*, \omega_u^*) = \ell_{cr}^*$. If $\ell_{cr}^* > \ell_{cr\,\max}$, then the required crank length exceeds its physical limit and is set to the maximal crank length $\ell_{cr\,\max}$.

The crank length feedback control adjusts the crank length of the IVT to achieve the desired output speed. The tracking error of the output speed of the IVT system, denoted as $\Delta\omega_u = \omega_u^* - \omega_u$, is used as the feedback variable. A proportional-integral control strategy is utilized to control the changing rate of the crank length, which can be represented as

$$\ell_{cr}(t) = \lambda_p\Delta\omega_u(t) + \lambda_i\int_0^t \Delta\omega_u(\tau)\mathrm{d}\tau \tag{4}$$

where λ_p and λ_i are the proportional and integral gains, respectively. The crank length generated by the crank length controller is used in the data-driven speed tracking controller to achieve the desired output speed of the IVT system.

To ensure that the tracking error $\Delta\omega_u$ asymptotically approaches zero, the crank length feedback control aims to achieve a stable and accurate control performance. By utilizing a combination of the crank length forward control and the crank length feedback control, the hierarchical speed control system can achieve the desired output speed of the IVT-based TCEC system and maintain its stability and efficiency under varying input conditions.

Overall, the hierarchical speed control system provides a robust and effective control strategy for the IVT-based TCEC system. The combination of the crank length forward control and the crank length feedback control ensures a stable and accurate control performance and enables the system to achieve the desired output speed and maintain its efficiency under varying input conditions.

4. DATA-DRIVEN OPTIMAL SPEED TRACKING CONTROL

In order to ensure the IVT system shown in Fig. 3 that has time-varying speed input can output a constant speed, an input speed controller needs to be designed to drive the DC motor to output the desire speed that is used for the crank length controller proposed in Sect. 3. In this section, we consider the DC motor and the noncircular gear pair as a whole system. We use a data-driven method to control the output speed of NG2 (ω_n) to track the desired speed value (ω_n^*) without building the dynamical model of the DC motor system.

Assume a general physical model that can describe the input-output relationship of the DC motor can be expressed as the following time-invariant form,

$$\dot{x}(t) = f(x) + g(x)u_p,\ x(t_0) = x_0 \tag{5}$$

where t_0 is the initial time, $x = [\theta_n, \omega_n]^{\mathrm{T}}$ is the state vector, $x_0 \in \mathbb{R}^2$ is the initial state, $u_p \in \mathbb{R}^1$ is the control voltage applied to the DC motor, $f(x)$ and $g(x)$ are continuous nonlinear functions. A cost function associated with the control input u_p is usually defined as

$$J = \int_{t_0}^{\infty}\{\mu^{\mathrm{T}}\left[f(x) + g(x)u_p - \dot{x}\right] + \mathcal{L}\left(x, u_p\right)\}\mathrm{d}\tau \tag{6}$$

where $\mathcal{L}(x, u_p) > 0$ is the Lagrange function and μ is the Lagrange multiplier. The necessary condition for J to achieve optimality is

$$\frac{\partial H(x, u_p, \mu)}{\partial u_p} = 0 \tag{7}$$

where $H = \mathcal{L}\left(x, u_p\right) + \mu^{\mathrm{T}}\left[f(x) + g(x)u_p\right]$ is the Hamiltonian function. According to the Pontryagin's minimum principle [12], the optimal output speed of the DC motor can be determined by $u_p^* = \arg\left\{\min_{\forall u_p \in U} H(x^*, u_p, \mu^*)\right\}$, where x^*, u_p^*, μ^* denote the optimal solutions and U is a bounded control subset that contains different controller candidate.

Define a value function

$$V(x) = \int_t^{\infty}\mathcal{L}(x, u_p)\mathrm{d}\tau \tag{8}$$

The Hamilton-Jocobi-Bellman (HJB) equation for the time-invariant system (5) can be written as

$$\mathcal{L}(x, u_p) + \frac{\partial V(x)^{\mathrm{T}}}{\partial x}[f(x) + g(x)u_p] = 0 \tag{9}$$

where $\frac{\partial V}{\partial x}$ plays the role of μ in the original definition of the Hamiltonian function. If $\mathcal{L}(x, u_p)$ is chosen to be $\mathcal{L}(x, u_p) = \frac{1}{2}(x^{\mathrm{T}}Qx + Ru_p^2)$ with $Q \ge 0$ a semi-positive matrix and $R > 0$ a positive number, the optimal speed control is

$$u_p^*(t) = -\frac{1}{R}g(x^*)\frac{\partial V(x^*(t))}{\partial x} \tag{10}$$

Then we use policy iteration method to update the value function to get its iterative solution. Let u_p^k and $V^k(x)$ denote the control input and value function at the k^{th} iteration, then we have

$$\frac{\partial V^{k+1}(x)^{\mathrm{T}}}{\partial x}\left[f(x) + g(x)u_p^k\right] + \mathcal{L}(x, u_p^k) = 0 \tag{11}$$

Let u_p' denote an admissible control at the $(k+1)^{th}$ iteration and substitute it into the expression for the derivative of $V(x)$ with respect to time, we have

$$\dot{V}^{k+1}(x) = \frac{\partial V^{k+1}(x)^{\mathrm{T}}}{\partial x}[f(x) + g(x)u_p'] \tag{12}$$

Subtracting Eq. (11) with Eq. (12), we get the following expression

$$\dot{V}^{k+1}(x) = -\mathcal{L}(x, u_p^k) + \frac{\partial V^{k+1}(x)^{\mathrm{T}}}{\partial x} g(x)(u_p' - u_p^k) \tag{13}$$

Besides, Eq. (10) implies that $\frac{\partial V^{k+1}(x)^{\mathrm{T}}}{\partial x} g(x)$ can be replaced by $-Ru_p^{k+1}$. So Eq. (13) can also be written as

$$\dot{V}^{k+1}(x) = -\mathcal{L}(x, u_p^k) - Ru_p^{k+1}(u_p' - u_p^k) \tag{14}$$

According to the integral reinforcement learning [15], integrating both sides of Eq. (14) from t to $t + \Delta t$, the following equation stands

$$\begin{aligned} &V^{k+1}(x(t)) - V^{k+1}(x(t+\Delta t)) \\ &-R\int_t^{t+\Delta t} (u_p^{k+1}(\tau)(\mathbf{u}'(\tau) - u_p^k(\tau))\mathrm{d}\tau \\ &= \int_t^{t+\Delta t} \mathcal{L}(x(\tau), u_p^k(\tau))\mathrm{d}\tau \end{aligned} \tag{15}$$

It is noted that the integral reinforcement learning algorithm is used to transform the differential Eq. (14) into an iterative algebraic equation in the form of Eq. (15) by introducing the input-output data of the system. Then the actor-critic form neural networks can be used to approximate the solution of Eq. (15). This approach has been widely used in data-driven control design process.

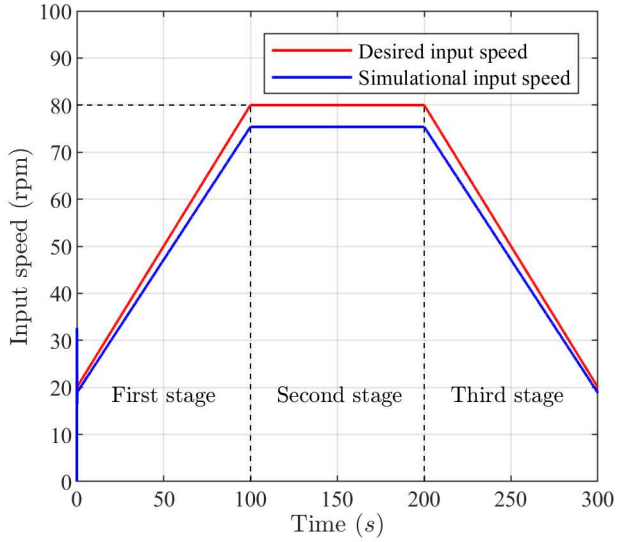

FIGURE 4: THE DESIRED INPUT SPEED AND THE SIMULATION INPUT SPEED UNDER THE PROPOSED CONTROL STRATEGY.

The optimal value function V^* and control policy u_p^* can be approximated through a critic neural network $\hat{V}^{k+1}(x) = \mathbf{w}_{V,k+1}^{\mathrm{T}}\boldsymbol{\phi}_V(x)$ and an actor neural network $\mathbf{u}^{k+1} = \mathbf{w}_{u,k+1}^{\mathrm{T}}\boldsymbol{\phi}_u(x)$ respectively, where $\boldsymbol{\phi}_V$, $\boldsymbol{\phi}_u$ are linearly dependent basis function vectors, and $\mathbf{w}_{V,k+1}$, $\mathbf{w}_{u,k+1}$ are the estimations of unknown coefficient vector. The system's states (or measurable outputs) are selected as the neurons of the actor network. The weighting parameters of each neuron are initialized to be zero and trained with the LS method based on the collected input-output data of the system.

Define a time sequence $t_j = j\Delta t$ with $j = 0, 1, \ldots, q$ for a large interval. Based on the least-squares (LS) principle, the estimated weighting function vector $\mathbf{W}_{k+1} = [\mathbf{w}_{V,k+1}^{\mathrm{T}}, \mathrm{vec}(\mathbf{w}_{u,k+1})^{\mathrm{T}}]^{\mathrm{T}}$ can be determined by minimizing the square of the residual $(e_j^{k+1})^2$. The solution of this LS problem is $\mathbf{W}_{k+1} = \left[\mathbf{P}^{\mathrm{T}}(\mathbf{W}_k)\mathbf{P}(\mathbf{W}_k)\right]^{-1}\mathbf{P}^{\mathrm{T}}(\mathbf{W}_k)\boldsymbol{\Pi}(\mathbf{W}_k)$, where $\mathbf{P}(\mathbf{W}_k) = \left[\rho_0, \rho_1, \ldots, \rho_q\right]^{\mathrm{T}}$ and $\boldsymbol{\Pi}(\mathbf{W}_k) = \left[\pi_0, \pi_1, \ldots, \pi_q\right]^{\mathrm{T}}$. Details can be found in [12, 16].

In this paper, the following basis function vectors are defined to be the hide layer neurons of the critic and actor NNs, $\boldsymbol{\phi}_V = [\theta_n^2, \omega_n^2, \theta_n\omega_n]^{\mathrm{T}}$, $\boldsymbol{\phi}_u = [\theta_n, \omega_n]^{\mathrm{T}}$. The initial weights $\mathbf{w}_{V0}$ and $\mathbf{w}_{u0}$ of the two NNs are set to zeros. The two weight matrices used to define the value function are set to $Q = diag([120, 0.1])$ and $R = 1.0$, respectively.

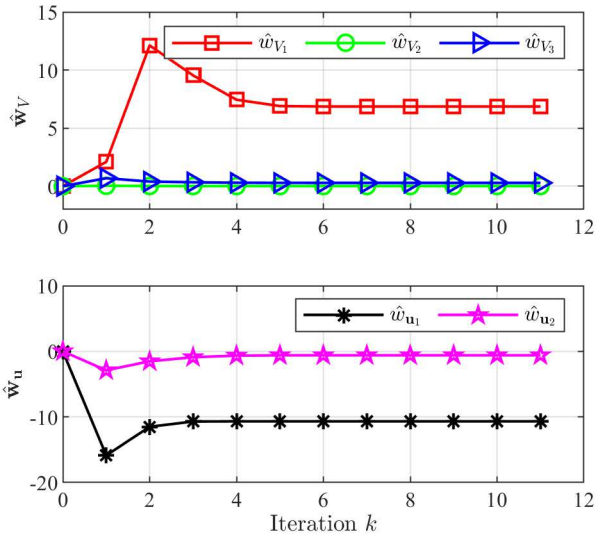

FIGURE 5: THE WEIGHT COEFFICIENTS OF THE CRITIC-ACTOR NEURAL NETWORKS IN THE TRAINING PROCESS.

5. SIMULATION RESULTS AND DISCUSSION

5.1 Simulation Results

In this section, we provide a scenario case to demonstrate the feasibility of the proposed control strategy. The tidal speed applied to the CFTs is assumed to be time-varying. Using Eq. (1), we can calculate the rotation speed of CFTs, which will be used as the input speed of the IVT system. Based on the speed ratio of the ICM, we can then solve for the rotation speed of NG2, denoted as ω_n, as shown by the red line in Fig. 4. The rotation speed can be divided into three stages - the first stage being a uniformly accelerating motion, the second one being a constant speed motion

stage, and the third one being a uniformly decelerating motion stage.

To obtain the optimal coefficients of the data-driven speed controller proposed in the previous section, the input and output data of the IVT system should be fed to neural networks. It is noted that the data are obtained from the dynamic model of the IVT system, which has been validated in the authors' previous works [8–10]. Then, the probing excitation signal is randomly chosen as $u_p(t) = 0.5(\sin(10.5\pi t) + \sin(24.5\pi t) + sin(38.5\pi t) + \sin(40.5\pi t) + \sin(55.5\pi t) + \sin(60.5\pi t) + \sin(75\pi t) + \sin(88\pi t))$ and the sampling time interval is set to be $\Delta t = 0.02$ s. By using u_p as the input voltage, we have measured the output state of the DC motor system based on the IVT's dynamic model, particularly the rotation angle and rotation speed of NG2. After 11 iterations, the coefficients of the NNs converge to $\mathbf{w}_V = [6.858, 0.0088505, 0.28439]$ and $\mathbf{w}_u = [-10.6773, -0.605826]$ respectively. The changing process of the weight coefficient of the neural network in the training process is shown in Fig. 5.

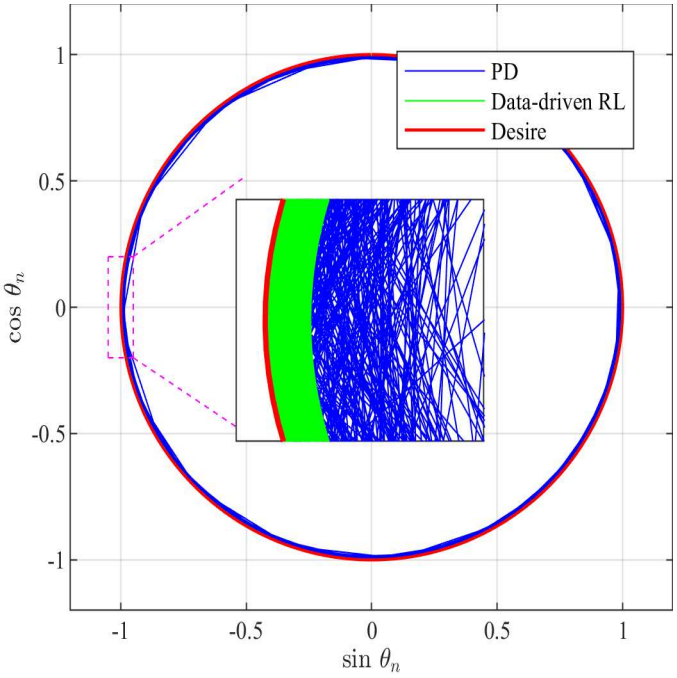

FIGURE 6: THE ROTATION ANGLE OF NG2.

Substituting the coefficients $\mathbf{w}_u$ of the 11^{th} iteration into $\mathbf{u}^{11} = \mathbf{w}_{u,11}^{\mathrm{T}} \boldsymbol{\phi}_u(x)$, we can use it to control the DC motor system and generate the tracking output speed signal, which is shown as the blue line in Fig. 4. However, we can observe that there is a significant speed-tracking error between the desired input speed and the simulated input speed. The maximum error is around 5.78%.

5.2 Discussion

We have studied the tracking performance of the rotation angle θ_n of NG2 by performing a coordinate transformation. The relationship between $\sin\theta_n$ and $\cos\theta_n$ is shown in Figure 6. The red line represents the corresponding angle at the desired speed ω_n^*, the green line represents the corresponding angle at the

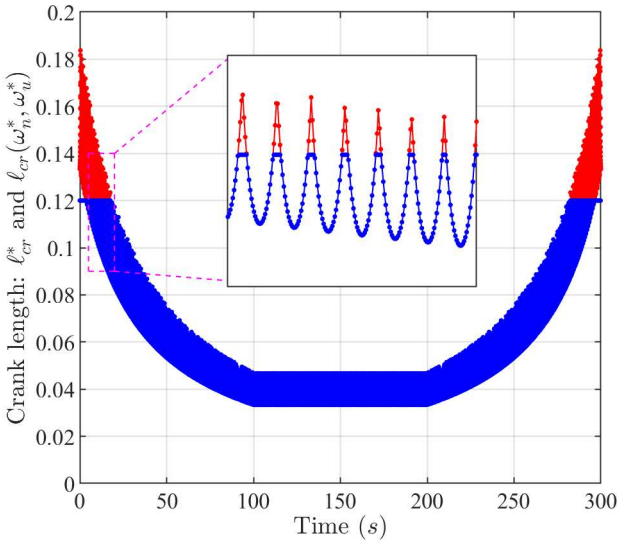

FIGURE 7: THE DESIRED CRANK LENGTH AND THE MODIFIED CRANK LENGTH FOR THE CRANK LENGTH CONTROLLER.

rotation speed under the data-driven RL control strategy, and the blue line represents the corresponding angle at the rotation speed under a traditional PD control. The figure shows that the proposed data-driven control approach has a significant advantage over the traditional control method in terms of tracking the rotation angle.

We then considered the desired rotation speed and the simulation rotation speed of NG2 under the proposed control strategy as the input speed to the IVT system, respectively, and studied the crank length control. We set the desired output speed of the IVT system to be $\omega_u = 70$ rpm and used the crank length controller to adjust the crank length in real-time to ensure that the output speed of the IVT system remains constant, regardless of the input speed. Using Eq. (3), we calculated the desired crank length ℓ_{cr}^* corresponding to the desired rotational speed of NG2. Then, taking into account the length constraint of the crank, we calculated a modified crank length $\ell_{cr}(\omega_n^*, \omega_u^*)$. Figure 7 shows the desired crank length and the modified crank length with respect to the desired input speed. It is evident that when the input speed is too slow, such as at the beginning and the end of the scenario case, a larger crank length is needed to adjust the input-output speed ratio to ensure the constant output speed of IVT.

Finally, we tested the output speed of the IVT system using the crank length controller. The simulation results for the output speed are shown in Fig. 8. The figure shows that the IVT system can successfully achieve a fixed speed output under the data-driven RL control for the DC motor and the crank length controller for the IVT system. However, there are significant fluctuations in the output speed of the IVT system, with an average error of about 5.48%.

6. CONCLUDING REMARKS

In summary, this paper proposes a new control strategy for the nonlinear control of the IVT system by combining a crank length control and a data-driven RL-based speed control. The input speed control is developed based on the sampling input-output

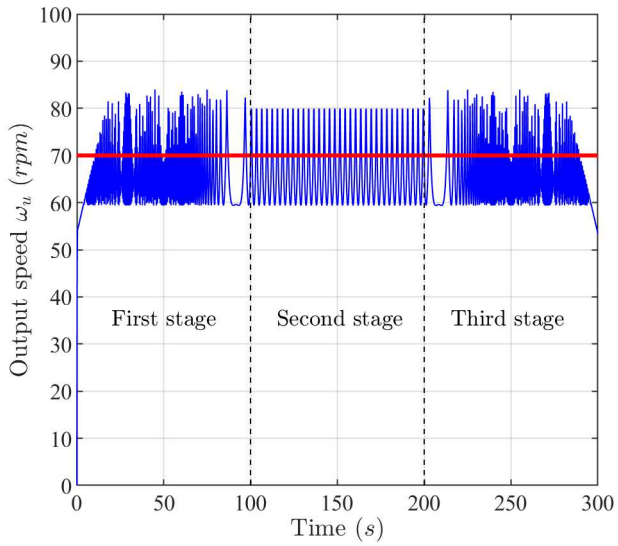

FIGURE 8: THE SIMULATIONS OUTPUT SPEED OF THE IVT SYSTEM UNDER THE PROPOSED CONTROL STRATEGY.

data of the IVT system rather than a dynamical model, which liberates the requirements for dynamic modeling processes. The crank length control is designed based on the physical mechanism of the IVT system. The proposed control strategy, along with the tracking error model, exhibits good control performance of the speed ratio of the IVT system with a variable input speed. The simulation results show that the control strategy can adjust and stabilize the speed ratio of the IVT system for the desired output speed. Although the output speed has large fluctuation errors, this study is only an initial exploration of the data-driven control method in TCEC speed control. The results show that this method has great application potential and has ample room for improvement. In the following research, we will try to carry out experimental research to verify the actual performance of the proposed control method.

ACKNOWLEDGMENTS

The first author is grateful for the financial support from the Natural Science Foundation of China under Grant No. 12302024. The second and third authors are grateful for the financial support from the National Science Foundation under Grant No. 2329791.

REFERENCES

[1] Pelc, Robin and Fujita, R. M. "Renewable energy from the ocean." *Marine Policy* Vol. 26 No. 6 (2002): pp. 471–479.

[2] Johnstone, C. M., Pratt, D. and Grant, J. A. Clarkeand A. D. "A techno-economic analysis of tidal energy technology." *Renewable Energy* Vol. 49 (2013): pp. 101–106.

[3] Li, G. and Zhu, W. D. "Tidal current energy harvesting technologies: A review of current status and life cycle assessment." *Renewable and Sustainable Energy Reviews* Vol. 179 (2023): p. 113269.

[4] Laws, N. D. and Epps, B. P. "Hydrokinetic energy conversion: Technology, research, and outlook." *Renewable and Sustainable Energy Reviews* Vol. 57 (2016): pp. 1245–1259.

[5] Lewis, M., Neill, S. P., Robins, P. E. and Hashemi, M. R. "Resource assessment for future generations of tidal-stream energy arrays, Energy." *Energy* Vol. 83 (2015): pp. 403–415.

[6] Li, G. and Zhu, W. D. "A Review on up-to-date gearbox technologies and maintenance of tidal current energy converters." *Energies* Vol. 15 No. 23 (2022): p. 9236.

[7] Wang, X. F. and Zhu, W. D. "Design, modeling, and experimental validation of a novel infinitely variable transmission based on scotch yoke systems." *Journal of Mechanical Design* Vol. 138 No. 1 (2016): p. 015001 (8 pages).

[8] Wang, X. F. and Zhu, W. D. "Design and stability analysis of an integral time-delay feedback control combined with an open-loop control for an infinitely variable transmission system." *Journal of Dynamic Systems, Measurement, and Control* Vol. 140 No. 1 (2018): p. 015001 (8 pages).

[9] Li, G., Wang, X. F. and Zhu, W. D. "Theoretical and experimental investigation on an integral time-delay feedback control combined with a closed-loop control for an infinitely variable transmission system." *Mechanism and Machine Theory* Vol. 164 (2021): p. 104410.

[10] Li, G. and Zhu, W. D. "Experimental investigation on control of an infinitely variable transmission system for tidal current energy converters." *IEEE/ASME Transactions on Mechatronics* Vol. 26 No. 4 (2021): pp. 1960–1967.

[11] Savaia, Gianluca, Sohn, Youngil, Formentin, Simone, Panzani, Giulio, Corno, Matteo and Savaresi, Sergio M. "Experimental automatic calibration of a semi-active suspension controller via bayesian optimization." *Control Engineering Practice* Vol. 112 (2021): p. 104826.

[12] Qin, Z. C., Zhu, H. T., Wang, S. J., Xin, Y. and Sun, J. Q. "A reinforcement learning-based near-optimal hierarchical approach for motion control: Design and experiment." *ISA Transactions* Vol. 129 (2022): pp. 673–683.

[13] Liu, Kai, Yu, Meilin and Zhu, Weidong. "Performance analysis of vertical axis water turbines under single-phase water and two-phase open channel flow conditions." *Ocean Engineering* Vol. 238 (2021): p. 109769.

[14] Liu, Kai, Yu, Meilin and Zhu, Weidong. "Enhancing wind energy harvesting performance of vertical axis wind turbines with a new hybrid design: A fluid-structure interaction study." *Renewable Energy* Vol. 140 (2019): pp. 912–927.

[15] Modares, H., Lewis, F. L. and Naghibi-Sistani, M. B. "Integral reinforcement learning and experience replay for adaptive optimal control of partially-unknown constrained-input continuous-time systems." *Automatica* Vol. 50 No. 1 (2014): pp. 193–202.

[16] Zhang, Q. and Zhao, D. "Data-based reinforcement learning for nonzero-sum games with unknown drift dynamics." *IEEE Transactions on Cybernetics* Vol. PP No. 99 (2018): pp. 1–12.